Effect of Specimen Size on the Dissipated Energy Density in Compression

Giuseppe Ferro[1]
e-mail: ferro@polito.it

Alberto Carpinteri

Department of Structural Engineering
and Geotechnics,
Corso Duca degli Abruzzi 24,
Politecnico di Torino,
10129 Torino, Italy

The size effects in compression on drilled cylindrical concrete specimens obtained from a unique concrete block over a large scale range (1:19) are analyzed. The experimental results show scale effects on dissipated energy density rather than on the compressive strength. A theoretical explanation for such a phenomenon is presented, assuming a noninteger physical dimension of the subdomain where dissipation occurs. A comparison between experimental and theoretical values is discussed and a renormalization procedure to obtain a scale-independent constitutive law is presented.
[DOI: 10.1115/1.2910899]

Keywords: compression test, concrete, dissipated energy density, size effects, microstructural disorder, fractals

Introduction

Scale effects have received a strong interest in the past few decades. With the term *scale effects*, both the variation of mechanical parameters and the variation of failure mode by varying the characteristic structural dimension (ductile to brittle transition) are considered. Very interesting results have been achieved by the second author in defining brittleness numbers, which easily determine the failure behavior: the static [1,2], the energetic [3–5], and the composite [6] brittleness number. In tension, the phenomenon has been deeply discussed and important conclusions have been set. In particular, the variation of tensile strength was considered with the formulation of different laws. Bažant [7] defined the so-called size effect law in the hypothesis of the presence of an initial crack of length proportional to the specimen size. This law has been often used in the literature. Successively, Carpinteri [8,9] and Carpinteri et al. [10] proposed the multifractal scaling law, valid for initially integer specimens and components. On the other hand, the compression failure is more complex and the related size effects are less understood.

The brittle failure in compression has been widely studied over the past decades. The phenomenon of axial splitting in the absence of confinement, as well as the related phenomena of exfoliation or sheet fracture, has been analyzed by Holzhausen and Johnson [11], by Nemat-Nasser and Horii [12], and by Ashby and Hallam [13]. Horii and Nemat-Nasser [14] have modeled the transition from brittle failure to ductile flow under very high confining pressures, by considering possible zone of plastically deformed materials at high shear-stress region around preexisting flaws. An interesting overview of brittle failure in compression can be found in Ref. [15].

Bažant and Xiang [16] proposed a simplified model of compression failure of quasibrittle columns, with the propagation of a band of axial splitting cracks in a direction parallel or inclined with respect to the column axis, predicting in that case the size effect on nominal strength. Rossi et al. [17], in order to explore the possibilities for the numerical modeling of concrete behavior, considered the failure of concrete in compression as the sequence of two-stage crack mechanisms. At the first stage, cracks parallelly open to the direction of loading, leading to the formation of slender columns in the material. At the second stage, these columns bend because of eccentric compressive loading and an oblique cracking mechanism starts at a scale smaller than the one of the columns. A softening branch is observed and, as a consequence, the multiscale heterogeneity of the material is proved to affect also the postpeak behavior. Markeset and Hillerborg [18] proposed the compressive damage zone model based on the hypothesis of compression failure mode as a combination of distributed axial splitting and localized deformation within a zone of limited length. Slate et al. [19] observed how the tensile mechanism is the most relevant crack mechanism controlling failure of concrete in uniaxial compression. In normal-strength concretes, they found highly irregular failure surfaces including a large amount of bond failure. In high-strength concretes, instead, the failure mode is that typical of nearly homogeneous materials in which failure occurs suddenly in a vertical, nearly flat plane passing through aggregates and mortar. This result can be easily explained by the model by Carpinteri and Chiaia [20], in which the fractal dimension of the fracture surface is presented as a function of aggregates and mortar characteristics.

The variation of the compressive strength with size and height-diameter (or slenderness) ratio is relevant when the rigid test machine platens are in direct contact with the concrete specimen, the lateral deformation of concrete being restrained at the specimen ends. In this context, a wide investigation has been carried out by Carpinteri et al. [21]. When, instead, the friction at the specimen ends is reduced, the strength variation is less evident.

Van Vliet and van Mier [22], using improved experimental techniques of axial displacement control and lubricated end platens as well as variable height to diameter ratios, observed that postpeak data from uniaxial compression experiments on plain concrete suggest a stress-displacement rather than a stress-strain relation. To obtain a unique empirical stress-displacement relationship, they suggested a functional dependence of the axial stress on the axial displacement, which turns out to be more or less insensitive to the height of the specimen.

An experimental investigation on geometrically similar cylindrical concrete specimens, obtained by a unique concrete block in compression over a very large scale range (1:19), will be briefly reported [23] and the obtained scale effects will be herein discussed. It will be shown how, avoiding friction, the strength is almost independent of specimen dimension while strong variations are observed for dissipated energy density. This phenomenon can be interpreted by considering the fragmentation and the com-

[1]Corresponding author.

Contributed by the Applied Mechanics Division of ASME for publication in the JOURNAL OF APPLIED MECHANICS. Manuscript received August 9, 2006; final manuscript received September 11, 2006; published online May 9, 2008. Review conducted by Robert M. McMeeking.

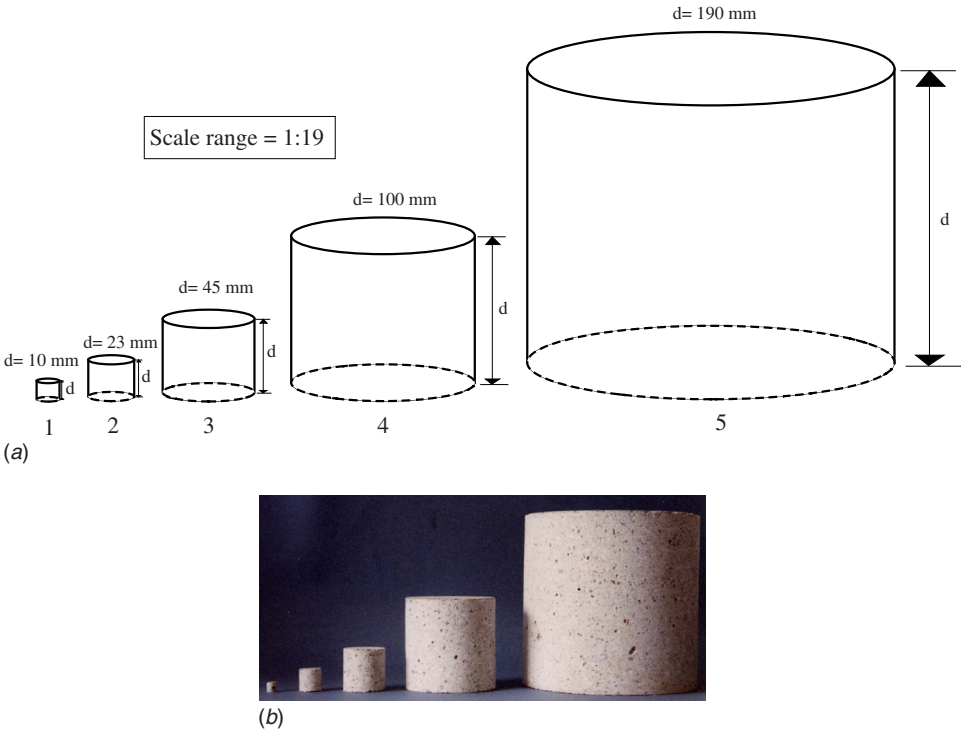

Fig. 1 (*a*) Geometries of the five different concrete specimens; (*b*) overall view of the five specimen sizes

minution theories. In this field, fractal geometry represents a very helpful tool to explain such a phenomenon. Turcotte [24] proposed a very interesting fractal approach for fragmentation. He affirmed that, if the fragments are produced over a wide range of sizes and if natural scales are not associated with the fragmented material, a fractal distribution of number versus size would seem to be expected.

In this context, a theoretical explanation, recently proposed by Carpinteri and Pugno [25,26], for the scale effects on the dissipated energy density in compression, is discussed and applied to the experimental results. From the theory, it can be evidenced how, in the scale range of the tested specimens, the energy dissipation occurs in a subdomain with a noninteger physical dimension.

In the last section, a scale-independent constitutive law in compression is put forward, which permits to define a unique relationship for softening in concrete. This goal is achieved by defining a fractal strain (or dilatation) whose fractal dimension is related to the subdomain in which energy dissipation occurs.

Experimental Evidence

In this section, the experimental tests performed at the Politecnico di Torino are briefly presented. As pointed out in the Introduction, all the cylinder were obtained on drilling from a unique concrete block with sizes $800 \times 500 \times 200$ mm^3. The microconcrete used for the specimens is characterized by a maximum aggregate size of 4 mm, with a compression strength, obtained by cubes ($150 \times 150 \times 150$ mm^3) after 28 days, equal to 33 N/mm^2. The water-cement ratio was equal to 0.65.

Five different diameters were considered in relation to the disposable drilling core bits in a scale range of 1:19. The specimens were cylinders with a height-diameter ratio $h/d=1$ and d chosen as characteristic dimension equal to 10 mm, 23 mm, 45 mm, 100 mm, 190 mm, respectively. Six specimens have been tested for $d=10$ mm, 23 mm, and 45 mm and four specimens for $d=100$ mm and 190 mm. The geometries of the tested specimens are presented in Fig. 1(a), while an overview of all the specimen sizes is reported in Fig. 1(b). Each specimen is individuated by a label formed by a letter C (compression) and by two numbers. The first number is related to the specimen dimension (1 for $d=10$ mm, 2 for $d=19$ mm, and so on) as reported in Fig. 1. The second number indicates the specimen.

For the three smallest sizes, the tests were carried out on a uniaxial compression machine with a capacity of 100 kN. The machine was controlled by a closed-loop servo-hydraulic system. All compression tests with this machine have been performed under displacement control, by imposing a constant rate of the displacement of the upper loading platen.

For the two remaining specimen sizes, $d=100$ mm (C4) and 190 mm (C5), a manual load controlled uniaxial compression machine with a capacity of 3000 kN was used. The choice of this kind of machine was necessary as the peak load for these specimens exceeded the maximum load of the other displacement controlled machines available in the laboratory. In addition, the height of the specimens did not permit the control of the postpeak load-displacement diagram, due to the more brittle structural behavior, unless a very sophisticated control system could be available, as performed by van Vliet and van Mier [22].

For these two larger sizes, loading cycles around the peak load were performed in order to capture the postpeak branch and to plot the entire curve. Unfortunately, as should have been easy to predict, only for one specimen (C44), we were able to capture the softening part.

The system adopted in the present compression tests for reducing friction at the ends of the specimens comes out from the analysis of the RILEM Technical Committee 148 SSC results [27]. These results suggested us to use two Teflon layers of 150 μm thickness with oil in between and a specimen slenderness equal to one.

The experimental load versus displacement diagrams can be found in Ref. [23]. Only one stress-deformation curve for each of the four sizes of concrete loaded in uniaxial compression is plotted in Fig. 2. These curves, as the load versus displacement ones, show a steadily initial increasing slope, due to the lower stiffness

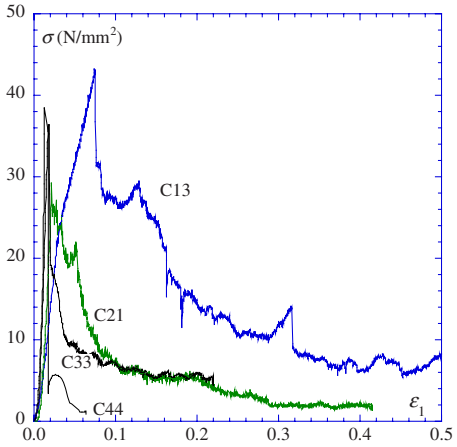

Fig. 2 Stress-strain curves for four different cylindrical specimen sizes

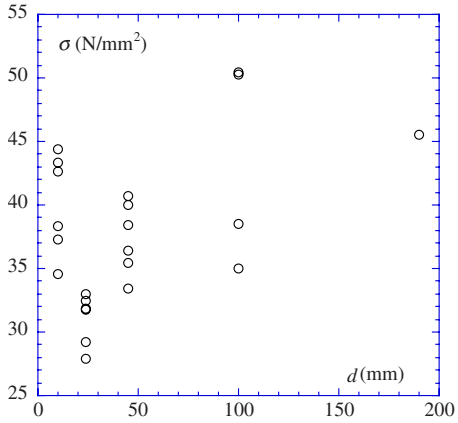

Fig. 4 Peak stresses by varying specimen size

at the beginning of the test, i.e., to the adjustment of the loading platens to the specimen surfaces and to the compressibility of the Teflon interlayers.

After this initial part, the stress-strain path is nearly linear and this linear part is as more pronounced as larger the specimen is (Fig. 2). The smaller the specimen, the more pronounced prepeak nonlinearities are. After the peak stress, a gradually descending branch has been detected. As it can be deduced from Fig. 2, the stress-strain curve for different specimens are almost the same in the prepeak regime, but, beyond the peak, the slope of the descending branch decreases with decreasing specimen height. Van Mier [28] plotted the normalized stress versus postpeak displacement diagrams, in which the displacements are calculated as

$$\delta = (\epsilon - \epsilon_{\text{peak}})h \tag{1}$$

and obtained nearly overlapping curves. He concluded that, as the same displacement is needed to fracture the specimens, the postpeak deformation must be localized in a small zone, and cannot be interpreted as an average strain. This fracture localization of concrete uniaxial compression implies that strain cannot be used as state variable in constitutive laws. The dimensionless stress versus postpeak deformation diagrams for four cylindrical specimen sizes are plotted in Fig. 3. It can be effectively evidenced that these curves are close to each other, even if different initial slopes, indicating an increase of brittleness with size, are present.

The values of the peak stresses, which are commonly called *compressive strength*, are reported in Fig. 4 by varying the specimen sizes. It can be noticed how, reducing friction, a marked size effect does not come out, as instead can be evidenced in tension [10,29,30] or in compression when localization is present [21]. The same results were obtained experimentally by the RILEM Committee 148 [27] and numerically by Carpinteri et al. [31,32] by simulations with a boundary element approach. The scatter in the results is not pronounced and even for the smallest size the values are comparable to the compressive strength of standard cubes. This permits to affirm that, if friction is avoided or drastically reduced, the compressive strength of an existing concrete structure can be evaluated using very small drilling core specimens.

The dissipated energy density can be evaluated by considering the area under the $P-\delta$ curve divided by the volume of the specimen. This is equivalent to consider the area under the stress-strain curve. The values of the dissipated energy density are plotted versus the characteristic specimen size in Fig. 9 in bilogarithmic plane. They undergo severe scale effects. The trend is a decrease by increasing the specimen dimension. This interesting result is discussed in the next section and a theoretical explanation is presented, based on a fractal hypothesis for the fragment size distribution generated during the compression test.

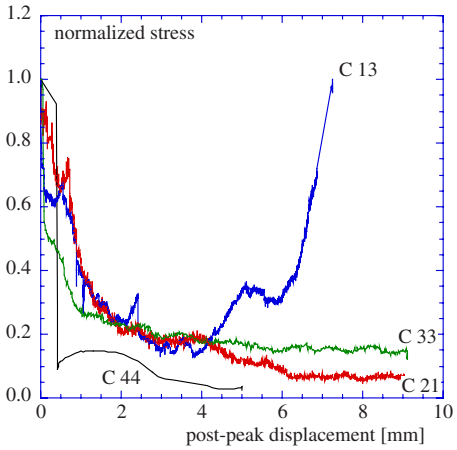

Fig. 3 Normalized stress versus postpeak displacement for four different cylindrical specimen sizes

Fractal Explanation of Size Effect on Dissipated Energy Density in Compression

Monofractal Approach. The performed compression tests have shown an evident decrease of dissipated energy density with increasing specimen dimension (Fig. 9). This interesting phenomenon can be interpreted by considering the fragmentation and the comminution theories. In this field, fractal geometry represents a very helpful tool. Fragmentation involves initiation and propagation of fractures. Fracture propagation is a highly nonlinear process requiring complex models even for the simplest configuration. Fragmentation involves the interaction between fractures over a wide range of scales. If fragments are produced over a wide range of sizes and if natural scales are not associated with the fragmented material, fractal distribution of number versus size would seem to be expected. The statistical number-size distribution for a large number of objects can be fractal [24,33].

Let us consider a concrete specimen, which undergoes a compression test. In the postpeak softening regime, the specimen is characterized by the generation of a large number of fragments. After fragmentation, the number of fragments N with a characteristic linear dimension greater than r should satisfy the relation

$$N = \frac{B}{r^D} \tag{2}$$

where B is a constant of proportionality, and D is the fractal

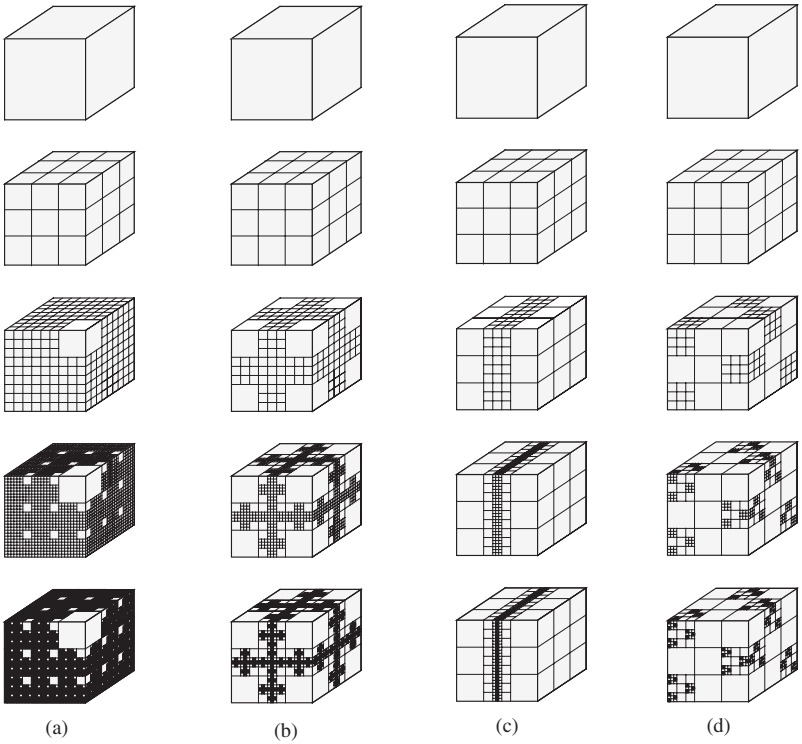

Fig. 5 Physical meaning of exponent *D*; (*a*) at each step, only one cube is retained, while all the others are divided into 27 equalsized cubes with $r_n = \frac{1}{3} r_{n-1}$ (*D*=2.93), very close to a volumetric fragmentation; (*b*) at each step, the eight angular cubes are retained, while all the others 19 are divided into 27 equal-sized cubes with $r_n = \frac{1}{3} r_{n-1}$ (*D*=2.70); (*c*) and (*d*) at each step, the nine cubes are divided into 27 equal-sized cubes with $r_n = \frac{1}{3} r_{n-1}$, while the others 18 are retained (*D*=2.00), showing a localization of the dissipation energy

dimension.

In order to describe the mechanical meaning of the fractal exponent D, in Fig. 5 some examples of discrete fragmentation model are presented, where fragmentation is a scale-invariant process that leads to a fractal distribution of chip sizes. We consider a fractal cube and use it as the basis for a fragmentation model. The fragmentation is such that some blocks are retained at each scale but others are fragmented. In order to determine D, Eq. (2) can be written as

$$D = \frac{\log(N_{n+1}/N_n)}{\log(r_n/r_{n+1})} \tag{3}$$

and then we can find for the three cases $D=\log 25/\log 3=2.93$ (Fig. 5(*a*)), $D=\log 19/\log 3=2.68$ (Fig. 5(*b*)), and $D=\log 9/\log 3=2.00$ (Figs. 5(*c*) and 5(*d*)), respectively. This is the fractal distribution of a discrete set. The cumulative number of blocks larger than a specified size for the three highest orders are $N_{1c}=2$ for $r_1=h/3$, $N_{2c}=52$ for $r_2=h/9$, and $N_{3c}=1302$ for $r_3=h/27$, obtaining a value $D=2.95$ for the first example; $N_{1c}=8$, $N_{2c}=160$, $N_{3c}=3048$, and $D=2.70$ for the second example; $N_{1c}=18$, $N_{2c}=180$, $N_{3c}=1638$, and $D=2.05$ for the last two (Fig. 6). The fractal dimensions for the discrete set and for the cumulative statistics are nearly equal.

Considering W as the global dissipated energy measured by the experimental setup, $\mathcal{G}$ as the elastic energy release rate or the specific energy necessary to generate the unit area of fracture, which is by hypothesis invariant with respect to the scale of observation, we have

$$W = \mathcal{G}A \text{ and then } \mathcal{G} = \frac{W}{A} = \frac{SV}{A} = \frac{Sl^3}{l^2} = Sl \tag{4}$$

If we consider a sequence of scale of observation, we have

$$\mathcal{G} = S_1 l_1 = \ldots = S_{n-1} l_{n-1} = S_n l_n = S_{n+1} l_{n+1} = \ldots = S_\infty l_\infty \tag{5}$$

where the first scale of observation could be the macroscopic one, with $S_1 l_1 = Sl$, l being the characteristic linear dimension of the specimen, and the asymptotic scale of observation could be the

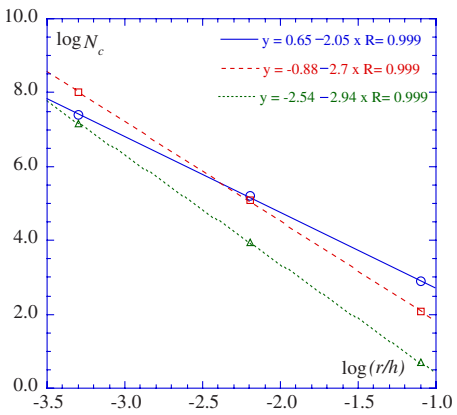

Fig. 6 Cumulative statistics for the proposed fragmentation models

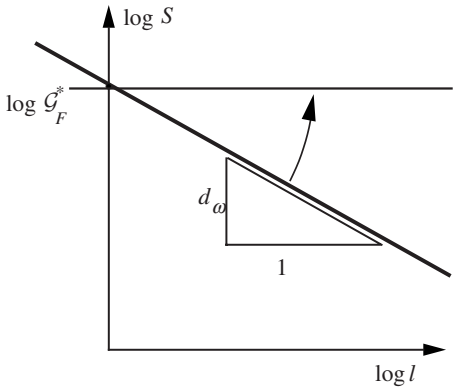

Fig. 7 Size effect on dissipated energy density in compression

microscopic one, with $S_\infty l_\infty = \mathcal{G}_F^* l^*$, l^* being the measure of the fractal set representing the fragmented configuration. From the equality between the extreme members, we can write

$$S = \mathcal{G}_F^*\left(\frac{l^*}{l}\right) \quad \text{or} \quad S = \mathcal{G}_F^*\left(\frac{l^{1-d_\omega}}{l}\right) \tag{6}$$

where $0 < d_\omega < 1$ is the decrement of the topological dimension due to the nonhomogeneous fragmentation. Taking the logarithms of both members of Eq. (6), we obtain

$$\log S = \log \mathcal{G}_F^* - d_\omega \log l \tag{7}$$

where $d_\omega = 3 - D$ can be considered as the decrement of the topological dimension of the set in which energy dissipation occurs. Equation (7) represents a straight line with slope $(D-3)$ in the $\log S$ versus $\log l$ plane (Fig. 7). If $D=2$, the slope is -1, as well as $D=3$ implies a vanishing slope. For $D=2$ (localization) $d_\omega = 1$; for $D=3$ (volumetric dissipation) $d_\omega = 0$.

The two extreme cases are $D=2$, surface theory [34], when the dissipation really occurs on a surface ($W \propto V^{2/3}$), and by $D=3$, volume theory [35], when the dissipation occurs in a volume ($W \propto V$). In this case, $\mathcal{G}_F^*$ presents the following physical dimensions:

$$[\mathcal{G}_F^*] = \frac{[F][L]^{-1}}{[L]^{D-2}} = [F][L]^{1-D} \tag{8}$$

For $D=2 \rightarrow [\mathcal{G}_F^*] = [F][L]^{-1}$, which is the canonical dimension for fracture energy, while for $D=3 \rightarrow [\mathcal{G}_F^*] = [F][L]^{-2}$, which is the physical dimension of stress. The experimental cases of fragmentation are usually intermediate ($D \cong 2.5$) [24], as well as the size distribution for concrete aggregates due to Fuller [36].

The fractal nature of the fragments generated by the compressive test emerges very clearly at the size scale of the specimens [37]. Momber [38] applied fragmentation theory to the study of compression and analyzed the fragments, determining a fractal exponent D close to 2. On the other hand, the property of self-similarity is very likely to vanish or change at higher or lower scales, owing to the limited characteristic of the particle size curve. The price to pay for obtaining a constant value is the loss of the classical physical dimensions for dissipated energy density. It is obviously very difficult to use these results in a structural analysis, a non-Euclidean (or fractal) mechanics being not yet available, even if very important steps have been moved forward by Carpinteri et al. [39].

Multifractal Approach. The monofractal hypothesis provides a dissipated energy density $S = W/V \rightarrow 0$ for $l \rightarrow \infty$. Due to the limited validity of the self-similarity property, this is of course a physical nonsense. The same trend has been obtained in traction [9,40], where the monofractal hypothesis was considered for cross-sectional ligaments. In that case, the geometrical multifractality of the cross-sectional material ligament [8,10] permitted to determine the multifractal scaling law for tensile strength, as well as for fracture energy [20,41] whenever the geometrical multifractality for fracture surface is assumed. The topological concept of geometrical multifractality, which can be also considered as an extension of the concept of self-affinity, may explain the inconsistencies shown in the preceding section. A self-affine fractal [42] is a fractal showing a different scaling law with respect to self-similarity, in the sense that a (statistically) similar morphology can be obtained only if the lengths are rescaled by direction-dependent factors. Such a fractal set can be identified by two different values of the fractal dimension: a local fractal dimension, in the limit of scales tending to zero, strictly equal to the Hausdorff topological dimension, and a global fractal dimension, corresponding to the largest scales, equal to the (integer) topological dimension.

On the other hand, as is shown in Fig. 8, it appears more consistent to deal with a continuous variation of the fractal dimension against the observation scale length (i.e., geometrical multifractality), than to consider only two limit values of the fractal dimension.

If a cube is fragmented in a recursive process into eight cubes (of $\frac{1}{2}$ linear dimension), at each step with probability f, the volume of each fragment and the number of fragments (cubes) at the nth step will be

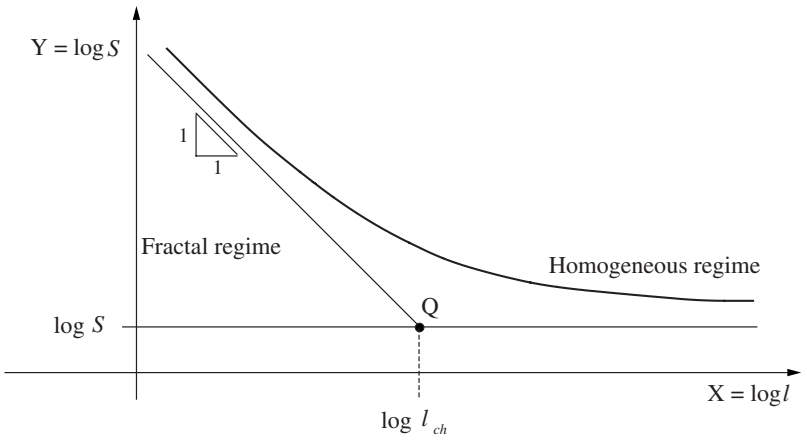

Fig. 8 Multifractal scaling law for volumetric energy dissipation versus size scale

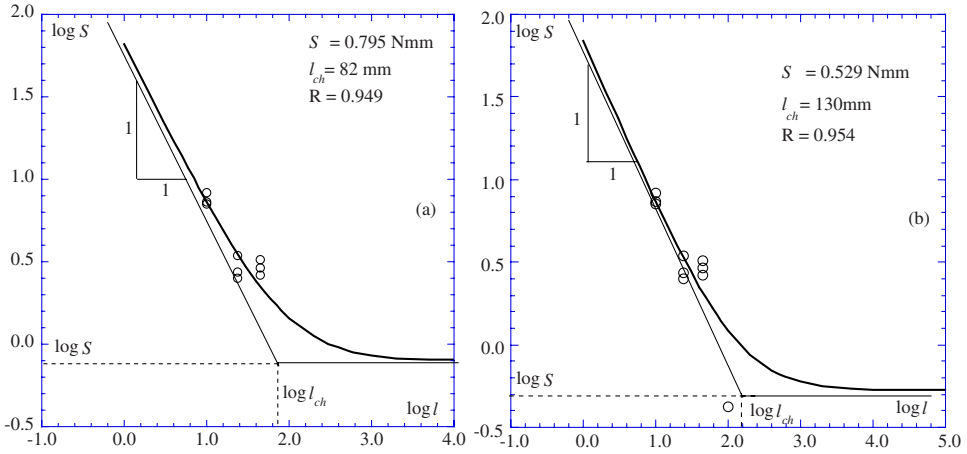

Fig. 9 Bilogarithmic diagrams of dissipated energy density versus size: (*a*) three sizes; (*b*) four sizes

$$V_n = \frac{1}{8^n} V_0 \tag{9}$$

$$N_n = (8f)^n N_0 \tag{10}$$

where V_0 is the volume of the N_0 original cubes. Taking the natural logarithms of both Eqs. (9) and (10) and eliminating n from them:

$$\frac{N_n}{N_0} = \left(\frac{V_n}{V_0}\right)^{-\ln 8f/\ln 8} \tag{11}$$

If a fragmented cube produces at each step a generic integer number V_0/V_1 of cubes, and noting that $V_n = r_n^3$, Eq. (11) can be generalized as

$$\frac{N_n}{N_0} = \left(\frac{r_n}{r_0}\right)^{-3\ \ln(V_0/V_1)f/\ln(V_0/V_1)} \tag{12}$$

From the comparison with the well-known definition of fractal distribution

$$N_n = \frac{B}{r_n^D} \tag{13}$$

it is possible to write

$$D = 3\frac{\ln \dfrac{V_0}{V_1} f}{\ln \dfrac{V_0}{V_1}} \tag{14}$$

From Eq. (14), we deduce the probability of fragmentation f (in any case greater than V_1/V_0):

$$f = \left(\frac{r_1}{r_0}\right)^{3-D} \tag{15}$$

In other words, assuming a constant probability f, we can describe a self-similar process and obtain a constant fractal exponent D. Carpinteri and Pugno [43] proposed the existence of a *material quantum* as a lower limit for chip size. This quantum is strictly related to the type of concrete considered. As affirmed by Slate et al. [19] for normal-strength concrete, it can be the aggregate, the fractures being irregular and only in the mortar or the interfaces mortar aggregate. For high-strength concrete, the quantum can be the sand grain, the fracture being more flat. This different quantum size justifes the translation of the law in Fig. 10. The probability of fragmentation should increase with fragment size and the corresponding exponent D should also increase according to Eq. (14). A nonconstant exponent D in Eq. (13) permits to describe a multifractal law [9]. The rupture of self-similarity in the fragmentation process should be due to the existence of the material quantum and represents the physical reason of the multifractal character. Carpinteri and Pugno [25,26,43] set that

$$D_{\min} = D(r = r_{\min}) \approx 2, \quad D_{\max} = D(r \to \infty) \approx 3 \tag{16}$$

as well as the corresponding probabilities are (Eq. (15))

$$f_{\min} = f(r = r_{\min}) = \frac{r_1}{r_0}, \quad f_{\max} = f(r \to \infty) = 1 \tag{17}$$

The simplest expression for f satisfying conditions (17) is

$$f(r) = \left(\frac{r_1}{r_0}\right)^{r_{\min}/r} \tag{18}$$

so that the following variation of D was obtained [25,26,43]:

$$D(r) = 3 - \frac{r_{\min}}{r} \tag{19}$$

allowing $D(r) \to 2$ for $r \to r_{\min}$, whereas $D(r) \to 3$ for $r \to \infty$.

According to the previous considerations, the following multifractal scaling law for dissipated energy density (Fig. 8) can be proposed [8,10,30]:

$$S = S_\infty \left(1 + \frac{l_{\text{ch}}}{l}\right) \tag{20}$$

where the two material constants S_∞ and l_{ch} can be obtained from fitting the experimental results. The physical requirements previously exposed are thus respected

$$\lim_{l \to +\infty} S_\infty \left(1 + \frac{l_{\text{ch}}}{l}\right) = S_\infty \tag{21}$$

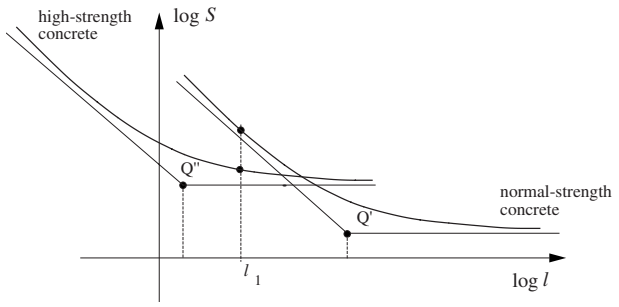

Fig. 10 Multifractal scaling law for two different material microstructures

$$\lim_{l\to 0^+} S_\infty\left(1+\frac{l_{ch}}{l}\right) = +\infty \tag{22}$$

In the bilogarithmic diagram shown in Fig. 8 ($X=\log l; Y=\log S$), the analytical expression becomes

$$Y(X) = \log S_\infty + \log\left(1+\frac{l_{ch}}{10^X}\right) \tag{23}$$

The asymptotes in the bilogarithmic plot present peculiar physical meanings (Fig. 8). The horizontal asymptote, corresponding to the larger sizes (*homogeneous* regime), presents the following expression:

$$H_1(X) = \log S_\infty \tag{24}$$

while the oblique asymptote, which corresponds to the macroscopic dimension l tending to zero (i.e., $X\to-\infty$) and governs the *disordered* or *fractal* regime, presents the following expression:

$$H_2(X) = -X + \log\sqrt{l_{ch}} \tag{25}$$

Point Q is the intersection of the two asymptotes (Fig. 8) and its horizontal coordinate is given by

$$X_Q = \log l_{ch} \tag{26}$$

where l_{ch} is a characteristic length. Point Q ideally separates the disordered regime, where fragmentation is not homogeneous, from the ordered (homogeneous) regime. The microstructural characteristic size l_{ch}, in the case of normal-strength concrete, could be proportional to the maximum aggregate size d_{max}:

$$l_{ch} = \alpha d_{max} \tag{27}$$

It is reasonable to suppose that for finer grained brittle materials (rocks, high-strength concrete), this value should be considerably smaller than in the case of normal-strength concrete, thus providing the curve to horizontally shift to the left in the bilogarithmic diagram (Fig. 10). Given a particular size l_1, for example, a normal-strength concrete specimen could behave according to the fractal disordered regime, whereas a rock or high-strength concrete specimen of the same size could be set in the (nearly) horizontal branch (Fig. 10), thus showing a homogeneous macroscopic behavior, characterized by a large and ordered distribution of microfractures.

The process shows two asymptotes. At the smallest scales, the dissipation occurs over a domain very close to a surface ($D=2$), whereas at the largest scales the dissipation occurs over a domain close to a volume ($D=3$).

Conclusions

The uniaxial compression tests performed under displacement control on drilled cylindrical specimens obtained by a unique concrete block over a very large scale range (1:19) have confirmed as that scale effect on compressive strength is not as evident as in traction. The experimental results have instead manifested a strong scale effect on dissipated energy density, showing a sharp decrease of that quantity by increasing specimen size.

The hypothesis of energy dissipation in a subdomain with physical dimension between 2 and 3 can be effective to justify such a phenomenon. It can be observed how, when energy dissipation occurs in the volume ($D=3$), no scale effects are present, whereas when energy dissipation occurs over an area ($D=2$), the scale effects are characterized in the bilogarithmic diagram $\log S$ versus $\log l$ by a linear law with slope equal to -1. By fitting the experimental values, we obtain an intermediate case, and a renormalized value for dissipated energy density, invariant with scale, can be obtained. This scale-invariant value is characterized by noninteger physical dimensions. This hypothesis works very well in the size range of the tested specimens.

In order to extend the trend of the dissipated energy density to all the size scales, a multifractal law has been proposed, from which comes out how at small scales the failure is dominated by a fragmentation process ($D=2$) with severe scale effect, while at large scales the energy dissipation occurs in the volume ($D=3$) and the related scale effect vanishes.

A renormalization procedure for strain (or dilation) has been eventually proposed in order to obtain a scale-invariant stress versus renormalized strain diagram.

Acknowledgment

The present research was carried out with the financial support of the Ministry of University and Scientific Research (MIUR) under the Grant No. PRIN 2003 "Damage mechanics and durability of ordinary and high performance concrete."

References

[1] Carpinteri, A., 1981, "Static and Energetic Fracture Parameters for Rocks and Concretes," Mater. Constr. (Paris), **14**, pp. 151–162.
[2] Carpinteri, A., 1982, "Notch Sensitivity in Fracture Testing of Aggregative Materials," Eng. Fract. Mech., **16**, pp. 467–481.
[3] Carpinteri, A., 1985, "Interpretation of the Griffith Instability as a Bifurcation of the Global Equilibrium," *Application of Fracture Mechanics to Cementitious Composites*, S. P. Shah, ed., Martinus Nijhoff, Dordrecht, pp. 287–316.
[4] Carpinteri, A., 1989, "Cusp Catastrophe Interpretation of Fracture Instability," J. Mech. Phys. Solids, **37**, pp. 567–582.
[5] Carpinteri, A., 1989, "Size Effects on Strength, Toughness and Ductility," J. Eng. Mech., **115**, pp. 1375–1392.
[6] Carpinteri, A., 1984, "Stability of Fracturing Process in R.C. Beams," J. Struct. Eng., **110**, pp. 544–558.
[7] Bažant, Z. P., 1984, "Size Effect in Blunt Fracture: Concrete, Rock, Metal," J. Eng. Mech., **110**, pp. 518–535.
[8] Carpinteri, A., 1994, "Scaling Laws and Renormalization Groups for Strength and Toughness of Disordered Materials," Int. J. Solids Struct., **31**, pp. 291–302.
[9] Carpinteri, A., 1994, "Fractal Nature of Material Microstructure and Size Effects on Apparent Mechanical Properties," Mech. Mater., **18**, pp. 89–101.
[10] Carpinteri, A., Chiaia, B., and Ferro, G., 1995, "Size Effects on Nominal Tensile Strength of Concrete Structures: Multifractality of Materials Ligaments and Dimensional Transition From Order to Disorder," Mater. Struct., **28**, pp. 311–317.
[11] Holzhausen, G. R., and Johnson, A. M., 1979, "Analyses of Longitudinal Splitting of Uniaxially Compressed Rock Cylinders," Int. J. Rock Mech. Min. Sci. Geomech. Abstr., **16**, pp. 163–177.
[12] Nemat-Nasser, S., and Horii, H., 1982, "Compression-Induced Nonplanar Crack Extension With Application to Splitting, Exfoliation and Rockburst," J. Geophys. Res., **87**, pp. 6805–6821.
[13] Ashby, M. F., and Hallam, D., 1986, "The Failure of Brittle Solids Containing Small Cracks Under Compressive Stress States," Acta Metall., **34**, pp. 497–510.
[14] Horii, H., and Nemat-Nasser, S., 1986, "Brittle Failure in Compression: Splitting, Faulting and Brittle-Ductile Transition," Philos. Trans. R. Soc. London, **319**, pp. 337–374.
[15] Nemat-Nasser, S., and Hori, M., 1993, *Micromechanics: Overall Properties of Heterogeneous Materials*, North-Holland, Amsterdam.
[16] Bažant, Z. P., and Xiang, Y., 1997, "Size Effect in Compression Fracture: Splitting Crack Band Propagation," J. Eng. Mech., **123**, pp. 162–172.
[17] Rossi, P., Ulm, F. J., and Hachi, F., 1996, "Compressive Behaviour of Concrete: Physical Mechanisms and Modeling," J. Eng. Mech., **122**, pp. 1038–1043.
[18] Markeset, G., and Hillerborg, A., 1995, "Softening of Concrete in Compression-Localization and Size Effects," Cem. Concr. Res., **25**, pp. 702–708.
[19] Slate, F. O., Nilson, A. N., and Martinez, S., 1986, "Mechanical Properties of High-Strength Lightweight Concrete," J. Am. Concr. Inst., **77**, pp. 606–613.
[20] Carpinteri, A., and Chiaia, B., 1995, "Multifractal Nature of Concrete Fracture Surfaces and Size Effects on Nominal Fracture Energy," Mater. Struct., **28**, pp. 435–443.
[21] Carpinteri, A., Ferro, G., and Monetto, I., 1999, "Scale Effects in Uniaxially Compressed Concrete Specimens," Mag. Concrete Res., **51**, pp. 217–225.
[22] van Vliet, M. R. A., and van Mier, J. G. M., 1996, "Experimental Investigation of Concrete Fracture Under Uniaxial Compression," Mech. Cohesive-Frict. Mater., **1**, pp. 115–127.
[23] Ferro, G., 2006, "Scale Effects on Compressive Tests for Concrete Specimens," Eng. Fract. Mech., **79**, pp. 1510–1530.
[24] Turcotte, D. L., 1992, *Fractals and Chaos in Geology and Geophysics*, Cambridge University Press, Cambridge.
[25] Carpinteri, A., and Pugno, N., 2002, "A Fractal Comminution Approach to Evaluate the Drilling Energy Dissipation," Int. J. Numer. Analyt. Meth. Geomech., **26**, pp. 499–513.
[26] Carpinteri, A., and Pugno, N., 2003, "A Multifractal Comminution Approach for Drilling Energy Dissipation," Powder Technol., **131**, pp. 93–98.
[27] van Mier, J. G. M., et al., 1997, "Report of the Round Robin Test Carried Out by RILEM TC 148-Ssc: Strain-Softening of Concrete in Uniaxial Compres-

sion," Mater. Struct., **30**, pp. 195–209.
[28] van Mier, J. G. M., 1986, "Multiaxial Strain-Softening of Concrete-Part 1: Fracture and Part II: Load-Histories," Mater. Struct., **19**, pp. 179–200.
[29] Ferro, G., 1994, "Effetti di Scala Sulla Resistenza a Trazione dei Materiali," Ph.D. thesis, Politecnico di Torino.
[30] Carpinteri, A., Chiaia, B., and Ferro, G., 1997, "A New Explanation for Size Effects on the Flexural Strength of Concrete," Mag. Concrete Res., **49**, pp. 45–53.
[31] Carpinteri, A., Ciola, F., and Pugno, N., 2001, "Boundary Element Method for the Strain-Softening Response of Quasi-Brittle Materials in Compression," Comput. Struct., **51**, pp. 389–401.
[32] Carpinteri, A., Ciola, F., Pugno, N., Gobbi, M. E., and Ferrara, G., 2001, "Size-Scale and Slenderness Influence on the Compressive Strain-Softening Behavior of Concrete," Fatigue Fract. Eng. Mater. Struct., **24**, pp. 441–450.
[33] Turcotte, D. L., 1986, "Fractals and Fragmentation," J. Geophys. Res., **91**, pp. 1921–1926.
[34] Rittinger, P. R., 1937, Lehrbuch der aufbereitungskunde. Berlin.
[35] Kick, F., 1885, Das gesetz der proportionalen widerstande. Leipzig.
[36] Stroeven, P., 1991, "Fractals and Fractography in Concrete Technology," *International Symposium on Brittle Matrix Composities*, Warsaw, Poland, pp. 1–10.
[37] Lee, Y.-H., and Willam, K., 1997, "Mechanical Properties of Concrete in Uniaxial Compression," ACI Mater. J., **94**, pp. 457–471.
[38] Momber, A. W., 2000, "The Fragmentation of Standard Concrete Cylinders Under Compression: The Role of Secondary Fracture Debris," Eng. Fract. Mech., **67**, pp. 445–459.
[39] Carpinteri, A., Chiaia, B., and Cornetti, P., 2001, "Static-Kinematic Duality and the Principle of Virtual Work in the Mechanics of Fractal Media," Comput. Methods Appl. Mech. Eng., **191**, pp. 3–19.
[40] Carpinteri, A., and Ferro, G., 1994, "Size Effects on Tensile Fracture Properties: A Unified Explanation Based on Disorder and Fractality of Concrete Microstructure," Mater. Struct., **27**, pp. 563–571.
[41] Carpinteri, A., and Chiaia, B., 1996, "Size Effects on Concrete Fracture Energy: Dimensional Transition From Order to Disorder," Mater. Struct., **29**, pp. 259–266.
[42] Mandelbrot, B. B., 1985, "Self-Affine Fractals and Fractal Dimension," Phys. Scr., **32**, pp. 257–260.
[43] Carpinteri, A., and Pugno, N., 2002, "Fractal Fragmentation Theory for Shape Effects of Quasi-Brittle Materials in Compression," Mag. Concrete Res., **54**, pp. 473–480.